

Non-Monotonic Thermoelectric Currents and Energy Harvesting in Interacting Double Quantum-Dots

Yair Mazal and Yigal Meir

*Department of Physics and the Ilse Katz Center for nanoscale Science and Technology,
Ben-Gurion University of the Negev, Beer Sheva, Israel*

Yonatan Dubi

*Department of Chemistry and the Ilse Katz Center for nanoscale Science and Technology,
Ben-Gurion University of the Negev, Beer Sheva, Israel*

(Dated: March 1, 2022)

A theoretical study of the thermoelectric current and energy harvesting in an interacting double quantum dot system, connected to reservoirs held at different chemical potentials and temperatures is presented. Using a rate-equation approach, the current is evaluated for different energetic configurations of the double quantum dot. We discuss in detail the current-temperature gradient relations (the thermoelectric analog to current-voltage relations), and demonstrate that, due to interactions, the current is non-monotonically dependent on thermal bias. This interaction-induced non-monotonicity influences the possibility of harvesting thermal energy from the double-quantum dot, and it is shown that in some configurations, energy cannot be harvested at all. We analyze the conditions under which energy can indeed be harvested and converted to useful electrical power, and the optimal conditions for thermoelectric energy conversion.

I. INTRODUCTION

In bulk systems, the efficiency of thermoelectric harvesting - generation of an electrical current and voltage from a temperature gradient - is limited by the material properties. The prospect of using nano-scale systems to enhance thermoelectric performance¹⁻³, along with the huge advances in constructing and manipulating nanoscale structures and devices, now make "nanoscale thermoelectrics" a large and interdisciplinary field of research. Indeed, nanoscale thermoelectric energy harvesting has now been demonstrated in systems such as nano-composite materials, carbon and silicon nanowires, Graphene nanostructures, molecular junctions, nanoparticles and quantum dots (see, e.g., Refs. 4-6 and references therein).

Besides the obvious applicative interest, in recent years it was realized that studying thermoelectric effects in nanoscale systems can shed light on the transport mechanisms dominating nanoscale structures. For instance, in molecular junctions, the thermoelectric voltage and thermopower can distinguish between different transport mechanisms⁷⁻⁹. Thermopower in quantum dots was studied over two decades ago, both theoretically and experimentally¹⁰⁻¹², with recent resurging interest focusing on role of interactions and non-linearity on thermoelectric efficiency¹³⁻²² (see review in, e.g., Ref. 23).

Double quantum dots (DQDs) are an excellent platform for studying the interplay between interactions, quantum effects (i.e. interference), charge and heat transport and thermoelectricity²⁴⁻³⁷. The possibility of arranging them in parallel or series, to couple them either by tunneling or capacitively, and to tune each quantum dot energy separately, gives rise to a large spectrum of parameters which can be tuned, leading to a broad spectrum of thermoelectric phenomena. Here, we study

the effect of DQD parameters (level spacing, interaction strength etc.) on thermoelectric energy harvesting. We focus on the non-linear response regime, with finite voltages and finite temperature difference. We show that at given temperature difference and finite bias, one cannot always harvest the thermal bias into electric power, and find the conditions for energy harvesting under different DQD parameters. We show that, surprisingly, in the presence of strong interactions such that transport is dominated by a single channel, there is a minimal temperature difference under which no harvesting is possible, and provide the mechanism for this effect.

The paper is organized as follows. In Sec. II the method and model are detailed. In Sec. III we discuss the dependence of current on temperature difference in the non-linear regime. In Sec. IV we discuss the conditions for energy harvesting, and Sec. V is devoted to summary and conclusions.

II. FORMALISM

A. Model

The system under consideration is a DQD, illustrated in Fig. 1. Within the DQD we take into account intra-dot as well as inter-dot Coulomb interaction. The DQD is coupled to two leads characterized by different temperatures and chemical potentials. The corresponding

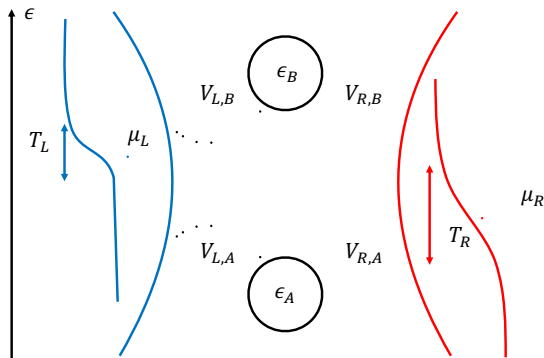


FIG. 1: An illustration of the system. We consider two levels with level spacing $\Delta\epsilon = \epsilon_B - \epsilon_A$. Each is connected to two leads ($V_{x,i}$), with possibly different temperatures $T_{L(R)}$ and chemical potentials $\mu_{L(R)}$.

Hamiltonian is:

$$\mathcal{H} = \sum_{\substack{k,\sigma \\ x=L,R}} \epsilon_{kx} c_{kx\sigma}^\dagger c_{kx\sigma} + \mathcal{H}_{DQD} + \sum_{\substack{k\sigma \\ i=A,B \\ x=L,R}} V_{kxi\sigma} c_{kx\sigma}^\dagger d_{i\sigma} + h.c., \quad (1)$$

where ϵ_{kx} is the energy of an electron with momentum k in the x -th lead ($x = L, R$), $c_{kx\sigma}^\dagger$ creates an electron with spin σ and momentum k in the lead, $d_{i\sigma}$ annihilates an electron with spin σ in the i -th dot, and $V_{kxi\sigma}$ is the coupling between the lead and the dot. The first term is the Hamiltonian of the leads, the second describes the DQD, and the third represents the interface. The Hamiltonian of the DQD can be written as:

$$\mathcal{H}_{DQD} = \sum_{\substack{\sigma, \\ i=A,B}} \epsilon_i d_{i\sigma}^\dagger d_{i\sigma} + U_0 \sum_{i=A,B} \hat{n}_{i\downarrow} \hat{n}_{i\uparrow} + U_1 \hat{n}_A \hat{n}_B, \quad (2)$$

where ϵ_i is the level of the i -th dot, U_0 (U_1) is the inter-dot (intra-dot) Coulomb interaction strength, $\hat{n}_{i\sigma} \equiv d_{i\sigma}^\dagger d_{i\sigma}$, and $\hat{n}_i = \hat{n}_{i\downarrow} + \hat{n}_{i\uparrow}$. All energies are measured from the zero-energy, defined as the energy of the empty dot. For simplicity, and to reduce the number of numerical parameters, we assume that $U_0 = U_1 = U$ ^{37–40}. One might expect that intra-dot Coulomb energy would be larger than inter-dot one. However, our results are valid as long as the inter-dot Coulomb interaction is not much smaller than the intra-dot interactions. Specifically (as we discuss in Sec. III), the interaction strength defines different transport regimes. Our results are thus qualitatively valid as long as U_0 and U_1 lie within the same regime.

The leads are modeled as free electron gases, and are characterized by their Fermi functions with temperatures $T_{L(R)}$, and chemical potentials $\mu_{L(R)} = \mu_{av} \pm \Delta\mu/2$. Without loss of generality we consider different temperatures such that $T_R > T_L$, and define the voltage as $\Delta\mu = \mu_L - \mu_R$, which can be either positive or negative.

B. Method

1. Rate Equations

When considering the Hamiltonian of Eq. 1 one may conceptually divide it into three parts: the DQD (system), the leads (reservoirs), and the tunneling between them. There are various ways to treat such systems, each has its advantages. In this work we use rate equations. Using rate-equation formalism, one finds the population of the system (diagonal elements of the density matrix) by solving a system of linear first-order differential equations. The standard procedure is to consider the steady state solution upon which the problem reduces to an algebraic system of linear equations whose solution, i.e. the kernel of the rate matrix, is the population of the DQD. The rate-equations are valid in the weak coupling limit which requires $\Gamma_{xij\sigma} \ll k_B T$ ^{41,42}, where $\Gamma_{xij\sigma}(\omega) = \sum_k V_{kxi\sigma} V_{kxj\sigma}^* A_{kx\sigma}(\omega)$, and $A_{kx\sigma}(\omega)$ is the spectral function. While generally $\Gamma_{xij\sigma}(\omega)$ is a function of energy (ω)^{42,43}, here we employ the wide band approximation, and assume constant density of states in the reservoirs within the relevant region of the spectrum, thus $\Gamma_{xij\sigma}(\omega) \cong \Gamma_{xij\sigma}$.

This approach is closely related to the master equations approach, and in fact they become the same at steady state for non-degenerate systems^{44,45}. However, rate equations can also be thought of as a consequence of time-dependent perturbation theory in first order (Fermi golden rule)⁴⁶, as a consequence of solving a many body Schrödinger equation⁴⁷, or as limiting case of Non-Equilibrium Green-Function approach when the width of the spectral function vanishes. The main advantage of the use of rate equations is that with relative ease one can model quite complex systems, which would require much more effort in other approaches, yet one is able to observe many of the interesting phenomena that such systems demonstrate. Additionally, they allow treatment of systems with competing energy scales with relative ease.

Within the rate-equation formalism we treat the DQD by diagonalizing \mathcal{H}_{DQD} (diagonal in position basis in our case), while the leads are treated as electronic reservoirs, and are characterized by their Fermi distributions. Electron transfer between the DQD and either lead is treated only within the rate matrix W whose elements are the rates for transition between eigenstates of the reduced (sub-)system which is the DQD. The rate equations read^{45,46,48}:

$$\frac{dp_m}{dt} = \sum_{\substack{n \\ n \neq m}} W_{n \rightarrow m} p_n - p_m \sum_{\substack{n \\ n \neq m}} W_{m \rightarrow n} \Leftrightarrow \dot{\mathbf{p}} = W \mathbf{p}, \quad (3)$$

where $W_{n \rightarrow m} = W_{mn}$ (for off-diagonal matrix elements) is the rate of transition from the many body Fock state $|n\rangle$ to $|m\rangle$, and p_m - the probability that the system will be in the many-body state $|m\rangle$ of the DQD. The rate

associated with adding an electron to the system is:

$$W_{n \rightarrow m} = \sum_{x=L,R} f(\epsilon_m - \epsilon_n - \mu_x) \times \quad (4)$$

$$\times \sum_{\substack{\sigma \\ i,j=A,B}} \Gamma_{xij\sigma} \langle m | d_{i\sigma}^\dagger | n \rangle \langle n | d_{j\sigma} | m \rangle,$$

while for removal of an electron the associated rate is:

$$W_{n \rightarrow m} = \sum_{x=L,R} \left(1 - f(\epsilon_n - \epsilon_m - \mu_x)\right) \times \quad (5)$$

$$\times \sum_{\substack{\sigma \\ i,j=A,B}} \Gamma_{xij\sigma} \langle m | d_{j\sigma} | n \rangle \langle n | d_{i\sigma}^\dagger | m \rangle,$$

where ϵ_m is the energy of the m -th state of the DQD, $f(\epsilon - \mu_x)$ stands for the Fermi function of the x -th lead, and therefore represents the probability of the lead to have an electron with the energy of the desired quasi-level and $\Gamma_{xij\sigma}$ (defined above) is the coupling of the DQD to the leads. The overlaps of the form $\langle m | d_{j\sigma} | n \rangle$ dictate whether the transition is allowed in the sequential tunneling regime, where allowed transitions move the system between states which differ by one electron. Eq. 3 also implies that the diagonal elements of the rate matrix read:

$$W_{mm} = - \sum_{\substack{n \\ n \neq m}} W_{m \rightarrow n} = - \sum_{\substack{n \\ n \neq m}} W_{nm}, \quad (6)$$

such that the sum of elements along each column vanishes. Steady state populations are found by solving $W\mathbf{p} = 0$, and imposing probability conservation ($\sum_m p_m = 1$).

2. Current

By defining the total particle number in the DQD as $\hat{n} = \sum_{i\sigma} \hat{n}_{i\sigma}$, we may find the particle current by writing:

$$\frac{d\langle \hat{n} \rangle}{dt} = \frac{d}{dt} \left(\sum_m n_m p_m \right) = \sum_m n_m \dot{p}_m = \sum_m n_m (Wp)_m =$$

$$= \underbrace{\sum_m n_m (W^L p)_m}_{\equiv J_L} + \underbrace{\sum_m n_m (W^R p)_m}_{\equiv J_R} = 0, \quad (7)$$

where $W = W^L + W^R$, and $W^{L(R)}$ is the matrix which corresponds to rates involving only the left (right) lead, and $n_m = \langle m | \hat{n} | m \rangle$ (since $[\hat{n}, \mathcal{H}_{DQD}] = 0$ the value of n_m is time independent as long as the leads aren't considered). At steady state, the latter is trivially $J_L + J_R = 0$, as the current flowing from the DQD to one lead, is exactly canceled by the current flowing into the DQD from

the other. However, if we only consider the current between the DQD and one of the leads the expression does not vanish and we can express the actual electric current flowing through the system by:

$$J = J^L = \frac{e}{\hbar} \sum_m n_m (W^L p)_m. \quad (8)$$

The power harvested by the DQD can simply be found by:

$$P_{out} = -J\Delta\mu. \quad (9)$$

In this work we express all energy scales in units of temperature. For quantum dots, typical operating temperatures range from millikelvins to room temperature, and our results consider temperatures of up to 1K, as this is the range of temperatures in which relevant experimental work²⁰ was conducted.

III. NON-MONOTONIC CURRENT-TEMPERATURE BIAS RELATIONS

We begin the results section of the paper by describing the non-trivial dependence of the current on the temperature bias. Similar to negative differential conductance (NDC), upon considering an interacting system with distinguishable transport channels ($\Delta\epsilon > T$), one may observe negative thermal response (NTR), seen as a non-monotonic dependence of J on thermal bias (ΔT). However, the mechanisms responsible for the two phenomena are not the same. As discussed in^{49,50}, in order to observe NDC one must consider unequal couplings between DQD and leads adhering to certain conditions. Even though NTR may be observed in the same regime, it may also be observed with equal couplings, as shown in recent theoretical studies^{24,51}, and experimental work²⁰ (which includes also a rate equations model), and is related to a dynamical channel blockade in quantum dots⁵².

Below, we discuss one of several configurations in which NTR is predicted in the presence of interactions, ranging from $U \sim \Delta\epsilon$ to strong interactions, $U \gg |\epsilon_{A,B}|, |\mu_{L,R}|, T$ (we measure energies and chemical potentials the empty dot, which is defined as zero energy), and with equal couplings. Due to the variety of parameters in our model, there are of course other configurations which may lead to the described phenomena. To give better intuition regarding the effect and to improve physical understanding, we try to shed light on the minimal requirements needed to observe the effect at the end of this section, and in appendix A.

Unlike previous works^{20,24,51}, we are motivated by potential applications regarding energy harvesting, and therefore consider also finite voltage ($\Delta\mu = \mu_L - \mu_R \neq 0$). To this end, J is plotted as a function of ΔT such that $T_L = T$, $T_R = T + \Delta T$. The thermal bias needed in order to observe the phenomena in the high temperature limit ($k_B T \gg \Gamma$), is rather large and challenging

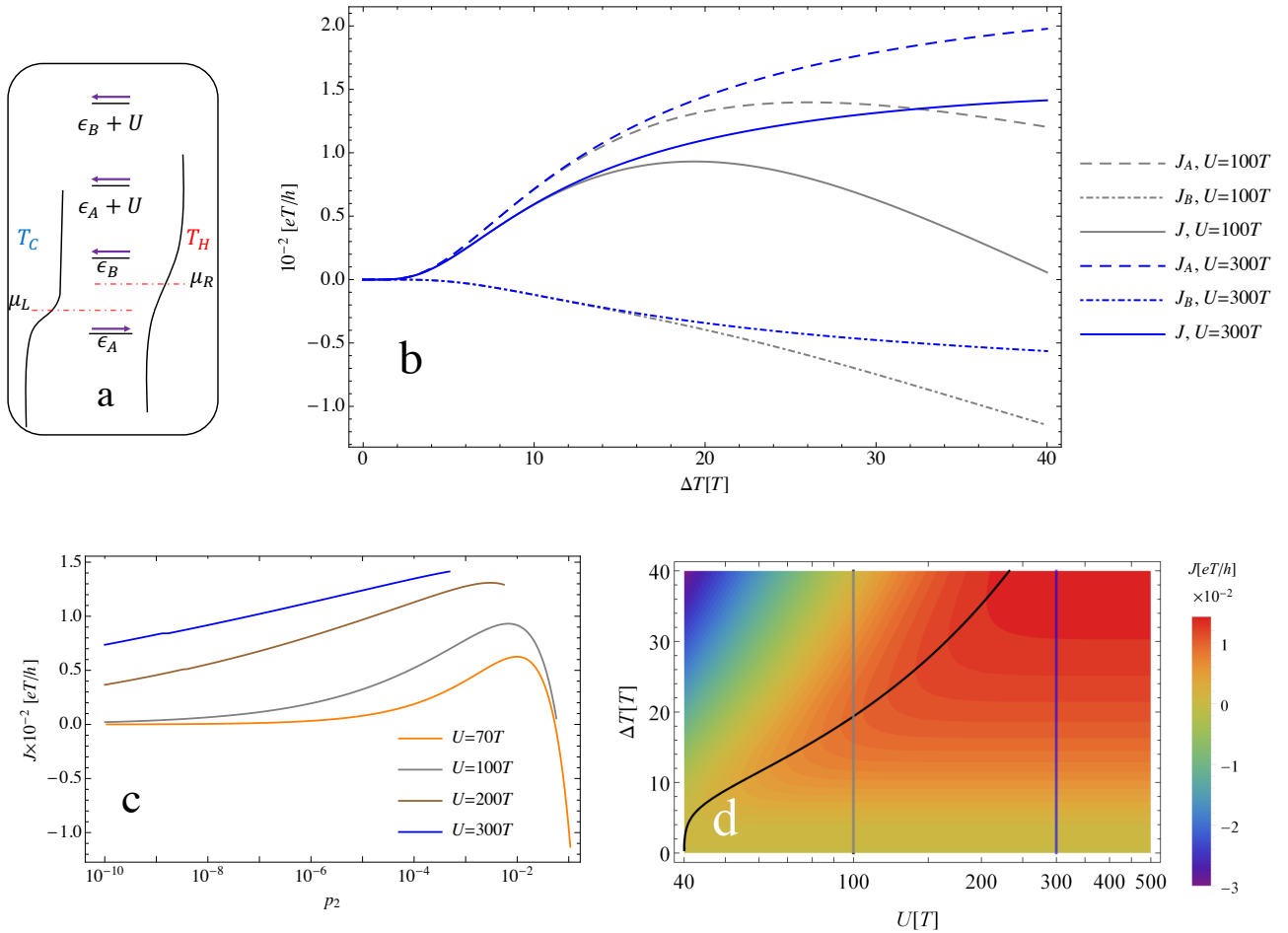


FIG. 2: (a) Illustration of transport channels alignments with the two chemical potentials $\mu_{L,R}$, where purple arrows indicate the direction of current through each channel. (b) Current through each dot ($J_{A,B}$) and total current ($J = J_A + J_B$) vs. the temperature difference ΔT for two values of the interaction strengths: $U = 100T, 300T$. (c) Current through the DQD (J), vs. probability of the DQD to contain two particles (p_2), for various values of U . (d) J vs. ΔT and U . The gray and blue vertical lines indicate values of U for which cross-sections were plotted in (b), while the black curve indicates the path along which the current has a local maxima (when plotted only against ΔT). Parameter values: $\Gamma = T/10$, $\epsilon_A = 10T$, $\epsilon_B = 40T$, $\mu_L = 20T$, $\mu_R = 30T$.

from an experimental point of view as discussed by²⁰, and our analysis assumes the maximal thermal bias as $\max(\Delta T) = 40T$ as reported in their work, though we predict the phenomena to be evident even for smaller thermal bias.

Fig. 2(a) illustrates the discussed configuration. It shows the alignment of leads with respect to accessible transport channels pertaining to single-particle states ($\epsilon_{A,B}$ in the figure), and to two-particle states ($\epsilon_{A,B} + U$ in figure), while purple arrows indicate the direction of current flowing through each channel upon sufficient heating of the right lead. Transport via single particle channels ($\epsilon_{A,B}$) occurs as an electron enters a previously empty system and then tunnels into the other lead. Transport via two-particle channels occurs as an electron tunnels into a system previously occupied with a single electron, thus requiring more energy ($\epsilon_{A,B} + U$) to tunnel into the system. Currents flowing through each dot ($J_{A,B}$) as well as total current ($J = J_A + J_B$) are plotted vs. thermal

bias for two interaction strengths in Fig. 2(b).

As expected, for $\Delta T = 0$ no current flows as there is no available channel within the Fermi window. A small thermal bias ($\Delta T \sim 5T$ in the figure) induces thermal current only through single-particle channels. However, current through the lower channel (illustrated as ϵ_A) prevails over current through the higher one (labeled as ϵ_B) for the following reason: since $f_{L,R}(\epsilon_B) \leq \frac{1}{2} \leq f_{L,R}(\epsilon_A)$ the probability of the system to be in Fock states with a single particle in dot A is necessarily larger than those with a particle in dot B as insertion and extraction rates are proportional to f and $1 - f$. Due to the interaction, these channels cannot support current simultaneously, and current through ϵ_A prevails. Note that this dominance is maintained even though we chose μ_R such that it is closer to ϵ_B , i.e. $|\mu_R - \epsilon_B| < |\mu_R - \epsilon_A|$, and thus one would expect naively the effect of ΔT on current flowing through ϵ_B to be greater.

For larger thermal bias, depending on the magnitude of

U , current may also flow through higher channels labeled as $\epsilon_{A,B} + U$ in Fig. 2(a). Current flowing through $\epsilon_B + U$ flows in the same direction as current through ϵ_B (since both $\epsilon_B, \epsilon_B + U > \mu_{L,R}$) and the two contributions add up. This is in contrast to current through ϵ_A and $\epsilon_A + U$ which flow in opposite directions (since $\epsilon_A < \mu_{L,R} < \epsilon_A + U$), which manifests in Fig. 2(b) as a local maxima in the gray dashed curve. The suppression of J_A together with the enhanced J_B are responsible for the local maxima in J in the solid gray curve. Since the position of the maxima in J vs. ΔT increases monotonically with U , the maxima in the blue line ($U = 300T$) is shifted to a value of ΔT beyond the domain depicted in the figure.

The Coulomb interaction determines the occupation of different levels. It is thus interesting to look at the correspondence between changes in current line-shape and the probability of the system to be in two-particle states. In Fig. 2(c) J is plotted vs. p_2 for various values of U , where p_2 is defined as sum of probabilities for being in any of the two-particle states. The curves were obtained by finding both J and p_2 for ΔT 's within the domain $\Delta T \in (0, 40T)$, and the curves terminate at the maximal allowed thermal bias, i.e. $\Delta T = 40T$ (intuitively, p_2 increases monotonically with ΔT). As shown, the current increases as a function of p_2 , up until a U dependent threshold, at which it drops sharply with the onset of the NTR. Quite surprisingly, Fig. 2(c) shows a huge sensitivity of the current to the occupations; a seemingly insignificant probability of 1% of the system to be in a two-particle state drastically alters transport, and is enough to cause NTR.

Fig. 2(d) shows the broader picture via a contour map of J vs. ΔT and U . The black curve shows the path along which the current has a local maxima for the specified $\Delta\epsilon, \mu_{L,R}$. The curve, which has been found numerically, illustrates approximately the minimal thermal bias required for NTR to be observed for a given value of U .

As expressed before, the specific setting under discussion is just one of many to cause non-monotonic current, and as shown in the appendix, it is predicted even for simpler systems. We wish to summarize here the basic requirements needed for non-monotonic dependence of current on thermal bias:

Alignment of Channels: The different behavior at finite thermal bias stems from competing current flow through different channels. Specifically, heating the electrode must create more electrons at an energy of one channel, while creating more holes at an energy of another. Thus, the chemical potential of the hot lead (μ_R) must be higher than the energy of some accessible transport channels ($\mu_R > \epsilon_A$ in Fig. 2(a)), and lower than others ($\mu_R < \epsilon_B, \epsilon_{A,B} + U$ in Fig. 2(a)).

Competition: Competition between currents flowing in opposite directions via different transport channels can contribute to stronger non-monotonicity (though, as shown in the appendix, this is not a

necessity). It happens if some channels are below both chemical potentials ($\mu_{L,R} > \epsilon_A$ in Fig. 2(a)), while others are above both ($\mu_{L,R} < \epsilon_B, \epsilon_{A,B} + U$ in Fig. 2(a)).

IV. ENERGY HARVESTING

Thermo-electric energy harvesting requires driving a current against a load, i.e. driving an electric current opposite to an external voltage ($\Delta\mu$) by means of a thermal bias (ΔT)²³. Harvesting systems can be classified as n-type if electric current flows from the hot lead to the cold one (same direction as heat flow), or as p-type if electric current flows from the cold lead to the hot one (opposite to heat flow)²³, and we discuss the required settings for each regime, limiting the discussion to equal coupling and strong interactions. We then consider also the case of weaker interaction strength ($U \sim \Delta\epsilon$).

A. Monotonic Harvesting, N-Type

Let us start with the case of very large (essentially infinite) U . For $\Delta\mu = \mu_L - \mu_R > 0$ energy harvesting requires $J < 0$ which occurs (approximately) when $f_R(\epsilon_A) > f_L(\epsilon_A)$. This is explained by the following: Trivially, the direction of current through dot A (J_A) depends solely on the above comparison. Similarly, the direction of current through ϵ_B is dictated by comparing $f_R(\epsilon_B)$ and $f_L(\epsilon_B)$. That being said, for $\epsilon_B > \mu_L$ the current through ϵ_A prevails over current flowing through ϵ_B , as, due to the strong interaction, the larger occupation of dot A prohibits occupation and current flow through ϵ_B . If, on the other hand, μ_L is assumed to be large enough such that occupations of the two dots are comparable, the currents through the two dots are similar too. Thus, in order to pass current against voltage (with $\Delta\mu > 0$ and strong interactions) we require: $f_R(\epsilon_{A(B)}) > f_L(\epsilon_{A(B)}) \Rightarrow f_R(\epsilon_A) > f_L(\epsilon_A)$, since, as explained, the condition regarding ϵ_B is obeyed trivially if the one for ϵ_A does.

The last inequality yields an analytic condition for harvesting:

$$\begin{aligned} f_R(\epsilon_A) > f_L(\epsilon_A) &\Rightarrow \frac{1}{e^{\frac{\epsilon_A - \mu_R}{T + \Delta T}} + 1} > \frac{1}{e^{\frac{\epsilon_A - \mu_L}{T}} + 1} \\ &\Rightarrow \Delta T > \Delta T_{harvest} = \frac{T(\mu_L - \mu_R)}{\epsilon_A - \mu_L} = \frac{2T\Delta\mu}{2\epsilon_A - \mu_{av} - \Delta\mu}. \end{aligned} \quad (10)$$

The above condition also contains another constraint, stating that for harvesting we must require $\epsilon_A > \mu_L$ as we consider $\Delta T > 0$ and $\Delta\mu = \mu_L - \mu_R > 0$. If this additional constraint is not obeyed, no amount of heating will cause current flow against the voltage (no harvesting) in the n-type regime with strong interactions (i.e. U is large enough to prohibit transport via two-particle channels).

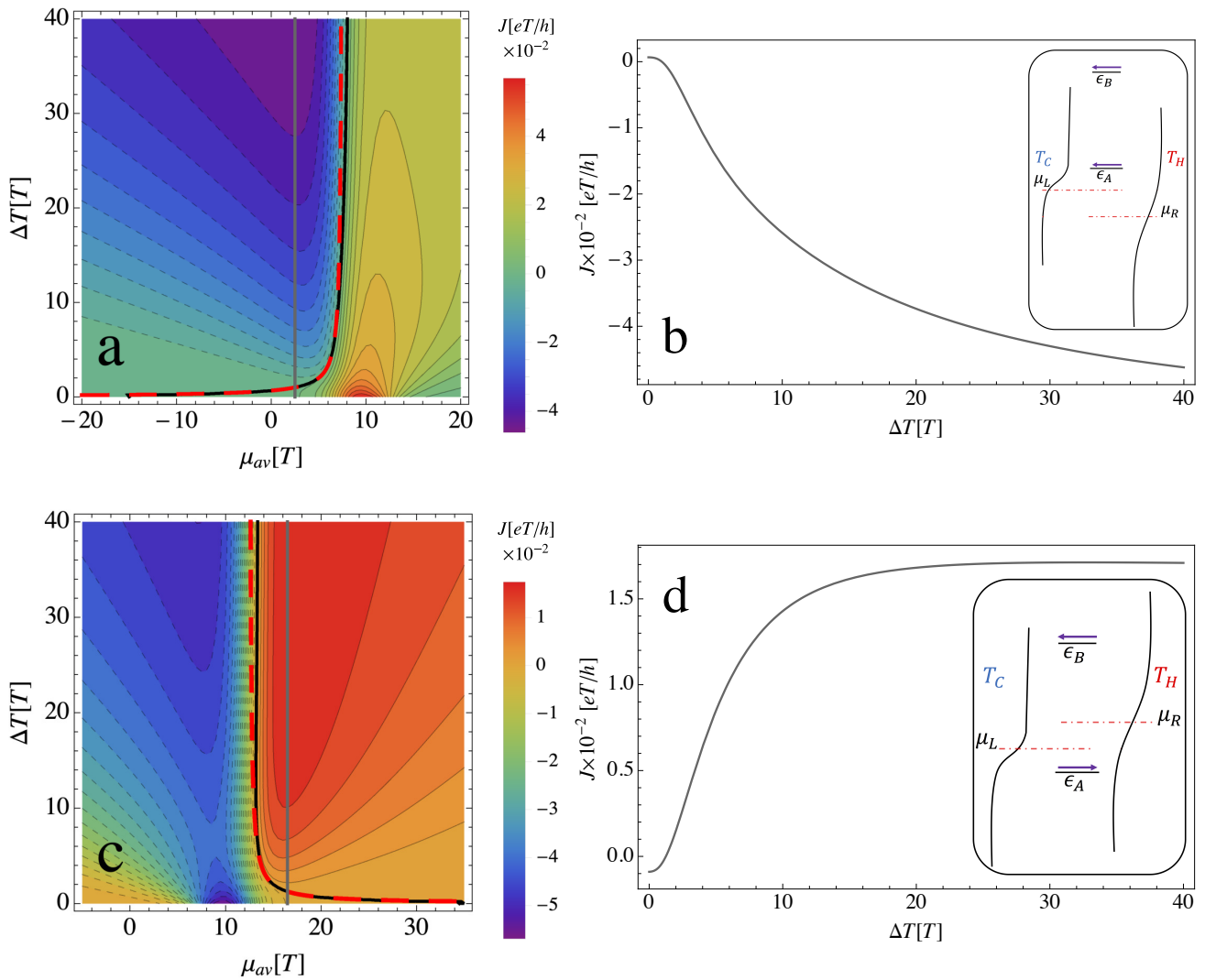


FIG. 3: (a) Contour plot of J vs. μ_{av} and ΔT for $\Delta\mu > 0$. The black curve indicates the contour line along which $J = 0$, the red curve plots Eq. 10 and the gray vertical line ($\mu_{av} = 2.5T$) indicates the path along which the cross section in (b) is taken. (c) Contour plot of J vs. μ_{av} and ΔT for $\Delta\mu < 0$. The black curve indicates the contour line along which $J = 0$, the red curve plots Eq. 10 and the gray vertical line ($\mu_{av} = 16.5T$) indicates the path along which the cross section in (d) is taken. Parameter values: $U = 1000T$, $\Gamma = T/10$, $\epsilon_A = 10T$, $\epsilon_B = 40T$, $|\Delta\mu| = 5T$.

Fig. 3(a) shows a contour plot of J vs. μ_{av} and ΔT for fixed $\Delta\mu$. Dashed contour lines indicate the domain in which current is negative (the DQD acts as a harvester, since $\Delta\mu > 0$), while solid contour lines indicate the domain of positive current, and the two are separated by the thick black curve indicating the curve along which current vanishes ($J = 0$). The thick red curve shows the analytic condition derived above (Eq. 10). As can be seen, the above condition approximates very well the black curve. The deviation at large ΔT stems from the fact that our derivation does not take in to account the less significant current flowing through ϵ_B .

Fig. 3(b) shows a cross section of the contour plot in Fig. 3(a) taken at $\mu_{av} = 2.5T$ as indicated by the vertical gray line in the contour map. In this regime the current is monotonic with respect to ΔT , in agreement with the

discussion in the previous section, as there is no competition between currents flowing in opposite directions. This is shown in the inset, which illustrates the alignment of the leads chemical potentials with the transport channels, with arrows indicating the direction of current flow through each channel upon heating of the right lead.

B. Monotonic Harvesting, P-Type

The DQD may also act as a p-type harvester and drive electric current from the cold lead to the hot one against a voltage, with the previous inequality merely changing direction, i.e. $f_L(\epsilon_A) > f_R(\epsilon_A)$. Therefore the relation in Eq. 10 still determines the cross-over between harvesting and investing energy, with the only change being that

now we consider $\Delta\mu < 0$, and thus the trivial condition switches to $\epsilon_A < \mu_L$.

Fig. 3(c) shows a contour plot of J vs. μ_{av} and ΔT , with dashed contours indicating negative current, and solid contours indicating positive current (here harvesting requires $J > 0$ as we consider $\Delta\mu < 0$). The two domains are separated by the thick black curve indicating the curve along which current vanishes ($J = 0$), while the thick red one shows the analytic approximation derived above (Eq. 10). As before, the red curve slightly deviates from the black one for large ΔT , stemming from neglecting the contribution to current through ϵ_B .

Fig. 3(d) shows a cross section of the contour plot in Fig. 3(c) taken at $\mu_{av} = 16.5T$ as indicated by the vertical gray line in the contour map. The inset illustrates the alignment of the leads chemical potentials with the transport channels, and the arrows indicate the direction of current flow through each channel upon heating of the right lead. Here too, the current is monotonic with respect to ΔT . Since the voltages taken into account in figures 3(b) and 3(d) are of the same magnitude, comparing current magnitudes reveals that for the discussed configurations the n-type regime allows for more power to be harvested.

C. Non-Monotonic Harvesting

1. Interaction Facilitated Harvesting

Allowing for a small enough interaction such that two-particle states may get occupied and current may flow through two-particle channels has trivial as well as surprising effects regarding harvesting. Trivially, as current flows through more channels the dominance of flow through ϵ_A is reduced, thus the analytic approximation employed before becomes less relevant. Another effect is that, if the bare levels are submerged in Fermi sea (single-particle channels are inaccessible), considering different strengths of interaction (U) may dictate whether the system harvests energy or not upon heating. This is easily seen in Fig. 4(a) which shows the power output, $P_{out} = I\Delta\mu$ vs. U and ΔT for an n-type configuration ($\mu_L - \mu_R = 5T$). As shown, the question whether or not the system harvests energy ($P > 0$, solid contour lines) depends on U and ΔT . More notably, there are values of U (for instance $U = 95T$ marked by a red vertical line in Fig. 4(a)) for which the system's behavior changes non-monotonically with ΔT between harvesting and investing energy (Fig. 4(b)).

2. Harvesting via Single-Particle Channels

When transport is dominated by current flowing through single-particle channels, interaction may either assist or hinder harvesting depending on configuration. To understand why this is the case, one must note that

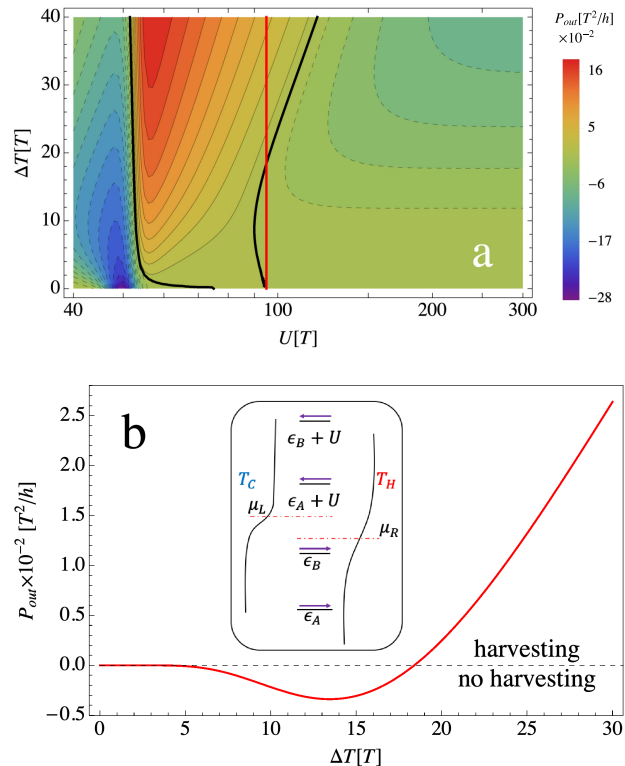


FIG. 4: (a) Contour plot of the output power P_{out} vs. U and ΔT . The black curves indicate the contour line along which $P_{out} = 0$, the red vertical line ($U = 95T$) indicates the path along which the cross section in (b) is taken. Harvesting occurs for $P_{out} > 0$ as indicated in the cross section. Parameter values: $\Gamma = T/10$, $\epsilon_A = 10T$, $\epsilon_B = 40T$, $\Delta\mu = 5T$, $\mu_{av} = 60T$.

in the n-type regime harvesting stems from current via channels which are aligned above the hot lead chemical potential ($\epsilon_i > \mu_R$), as illustrated in Fig. 3(b). On the other hand, in the p-type regime, harvesting stems from current via channels which are beneath the hot lead chemical potential ($\epsilon_i < \mu_R$), as illustrated in Fig. 3(d). This is shown in Fig. 5, where the output power P_{out} (Eq. 9) is plotted as a function of ΔT for opposite voltages (n-type and p-type regimes), and for two interaction strengths, $U = 45T, 300T$. The relevant configuration is the same as the one illustrated in Fig. 2(a). As seen, in the n-type regime ($\Delta\mu > 0$) the two-particle channels assist harvesting and in fact if U is too large harvesting is impossible in this configuration as the two-particle channels are blocked. On the other hand, in the p-type regime ($\Delta\mu < 0$), the interaction hinders harvesting, and therefore if the interaction is small enough to allow two-particle channels to affect transport, harvesting is possible only for a limited (U dependent) range of thermal bias.

3. Maximal power and optimal thermal bias

As implied from the previous discussion, under given conditions (negative bias, so called p-type regime, and intermediate interaction strength) the power output displays non-monotonic behavior as a function of the thermal bias. This needs to be accounted for, if one wishes to optimize the performance of the thermoelectric device as an energy harvester. To explore this situation, we have performed the following computation. A set of DQD systems, all with the same energies, average chemical potential and couplings, but with different interaction strengths ($30T < U < 150$) were considered ($\epsilon_A = 10T, \epsilon_B = 40T, \mu_{av} = 25T, \Gamma = T/10$). The bias voltage was scanned in the range $-20T < \Delta\mu < -T$. For each system (value of U) and each voltage bias ($\Delta\mu$), the temperature bias ΔT for which one obtains maximal power was found. Each point in Fig. 6 depicts that maximal power as a function of the optimal thermal bias for the different voltage biases, and a given value of U . The different curves correspond to different interaction strengths, according to the color coding.

The first thing one notices is that the larger the interaction strength, more power can be extracted at optimal conditions. This is easy to understand; in the discussed setting, the harvested current passes through the lower transport channel (ϵ_A). The current that flows through two particle channels (at energies $\epsilon_{A(B)} + U$), in the direction of the voltage bias (suppressing harvesting), is diminished by the increasing interaction.

Second, for each value of U there is an optimal thermal bias (ΔT_{opt}) which maximizes the harvested power. The exact ΔT for which power is maximal has a non-trivial dependence on U , and in fact, as discussed in the appendix, even for a non-interacting system the maximum of harvested power has no simple analytic form.

Third, one can observe a specific structure of the data; for each value of U there is a well-defined "trajectory" when plotted against ΔT_{opt} . The inset shows one ex-

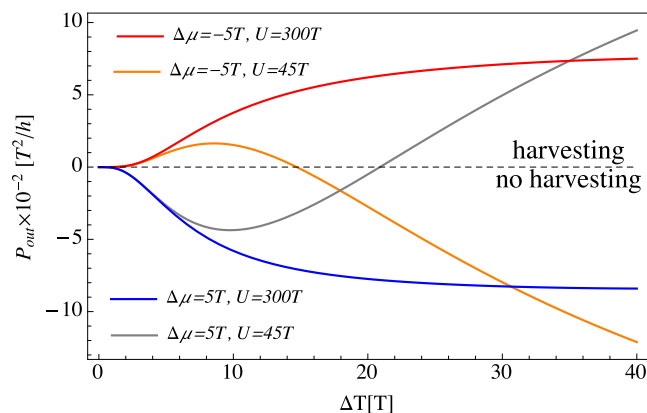


FIG. 5: P_{out} vs. ΔT for given values of $\Delta\mu$ and U . $P_{out} > 0$ means that the system harvests energy. Parameter values: $\Gamma = T/10, \epsilon_A = 10T, \epsilon_B = 40T, |\Delta\mu| = 5T, \mu_{av} = 25T$.

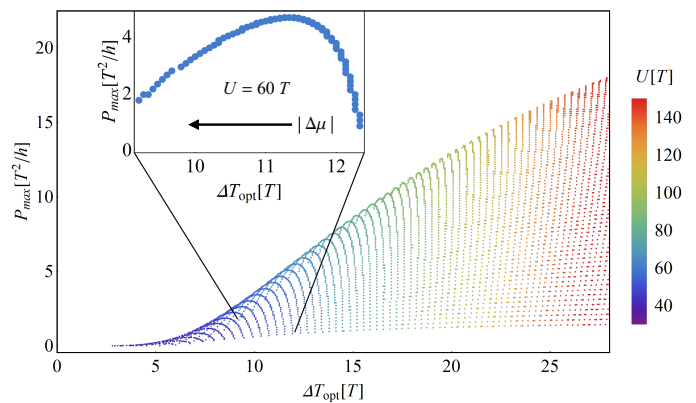


FIG. 6: Maximal power output P_{max} plotted against optimal temperature difference ΔT_{opt} , calculated for different voltage biases and interaction strengths (see text for numerical parameters). The key observation is that, as opposed to non-interacting system, there is an optimal bias voltage and temperature difference for which power output is maximal: selected data set for $U = 60T$, showing the power-temperature non-monotonic curve.

ample of such a trajectory (taken at $U = 60T$), in the $\{P_{max}, \Delta T_{opt}\}$ plane. The arrow indicates the direction of increasing negative voltage, from $\Delta\mu = -1T$ to $\Delta\mu = -20T$. Maximal power appears at $\Delta\mu \sim -11T$. In general, the optimal power must depend on the applied voltage. This is in contrast with the strong- U case (as in Fig. 3), where one expects a monotonic dependence on voltage. For the (intermediate) interacting case, on the other hand, the non-monotonicity in the current implies a more subtle relation between optimal power, optimal thermal bias and voltage bias, depicted in Fig. 6. This point should be considered for optimal design of an experimental apparatus.

V. SUMMARY AND CONCLUSIONS

To summarize, in this work we studied the thermoelectric current and energy harvesting in an interacting double-quantum-dot system, connected to reservoirs held at different chemical potentials and temperatures. Using a rate-equation approach, the current was evaluated for different energetic configurations of the DQD. We discuss in details the current-temperature gradient relations (the thermoelectric analog to current-voltage relations) and the conditions under which energy (from the temperature gradient) can be harvested and converted to useful electrical power.

Specifically, our main results are: (i) In the presence of interactions, the current-thermal bias relations may exhibit non-monotonic behavior, in analogy to negative differential conductance in voltage-biased interacting quantum dot junctions. (ii) there is an extreme sensitivity of the current to the populations on the dot. Specifically, a tiny change in the quantum dot occupations can alter qualitatively the current-bias voltage dependence. (iii) Energy harvesting can be enhanced or hindered by

Coulomb interactions, depending on the specific conditions of the DQD. (iv) In the presence of interactions, the non-monotonic current leads to non-trivial optimal configuration of the DQD. More specifically, one can say that it is not always the case that the larger the thermal bias the more energy can be harvested.

These results provide insight into the nature of thermoelectric transport in quantum-dot junctions. Being well within current experimental capabilities, our predictions can be tested experimentally. Going beyond the weak-coupling limit, extending the system to more than two quantum dots, and allowing for direct coupling between the quantum dots (i.e. electron tunneling between the dots) are all directions we plan to address in the future.

ACKNOWLEDGMENTS

YM acknowledges support from ISF grant 292/15. YD acknowledges support from ISF grant 1360/17.

Appendix A: Minimal Models for Non-Monotonic Current

In this appendix we address the question of what are the minimal requirements for non-monotonic current. We demonstrate similar phenomena to those discussed in the text can be expected for simpler systems, depending upon proper tuning of the system parameters.

1. Single Interacting QD

For a single, spinful QD (SQD), with Coulomb repulsion between spin-degenerate states, the Hamiltonian reduces to:

$$\mathcal{H}_{QD} = \sum_{\sigma} \varepsilon d_{\sigma}^{\dagger} d_{\sigma} + U \hat{n}_{\downarrow} \hat{n}_{\uparrow}. \quad (\text{A1})$$

Since the system still contains two transport channels (at energies ε and $\varepsilon + U$), aligning the chemical potential of the leads as specified in Sec. III such that $\varepsilon < \mu_R$ and $\varepsilon + U > \mu_R$, the current $J(\Delta T)$ versus finite thermal bias (ΔT) is non-monotonic. This is shown in Fig. 7, which shows the current flowing through the QD vs. ΔT , with an illustration of the alignment of transport channels with respect to the chemical potentials of the leads in the inset.

2. Non-Interacting DQD

If one considers a non-interacting DQD the Hamiltonian reduces to:

$$\mathcal{H}_{DQD} = \sum_{i=A,B} \varepsilon_i d_i^{\dagger} d_i \quad (\text{A2})$$

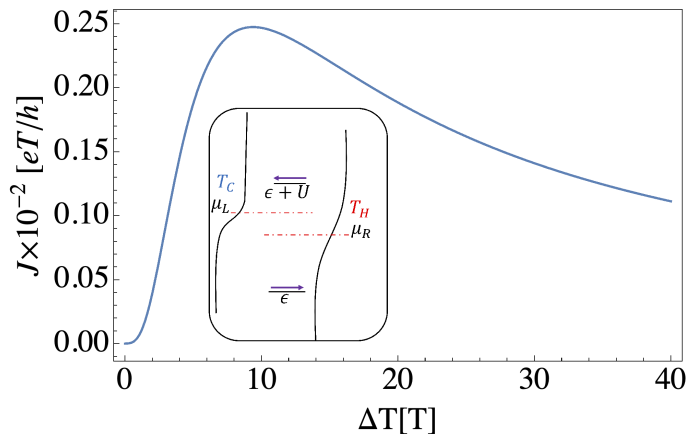


FIG. 7: Current flowing through the QD vs. ΔT . The inset illustrates the alignment of transport channels with respect to the chemical potential of the leads. Parameter values: $U = 30T$, $\Gamma = T/20$, $\varepsilon = 10T$, $\mu_L = 28T$, $\mu_R = 22T$.

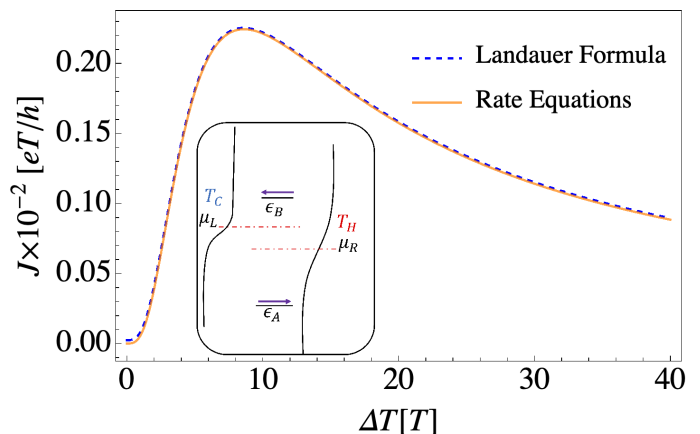


FIG. 8: Current flowing through the DQD vs. ΔT . The orange curve was obtained using rate equations, and the blue dashed curve was obtained by using Landauer formula. The inset illustrates the alignment of transport channels with respect to the chemical potential of the leads. Parameter values: $\Gamma = T/20$, $\varepsilon_A = 10T$, $\varepsilon_B = 40T$, $\mu_L = 28T$, $\mu_R = 22T$.

The spin degree of freedom has been omitted from the above Hamiltonian as we wish to compare the following results with the results of the single QD case presented before. Therefore we wish to consider a system which can contain up to two electrons simultaneously, at one of two energy levels.

As long as we consider a non-interacting system we can treat it either by the rate-equation formalism utilized throughout this work, or by Landauer formula. Following the work of 53, an expression for the transmission similar to theirs can be obtained, as well as an expression for current in terms of digamma functions.

Figure 8 shows the current flowing through the non-interacting DQD vs. ΔT . The figure shows results using both rate equations and Landauer formula based expressions. As shown, since we consider weak coupling limit ($\Gamma \ll K_B T$), the results are equivalent. Unlike the results of 53 we do not limit ourselves to linear response.

3. Roles of Interactions

To understand the effect of interaction on the system, in figure 9 we plot J vs. ΔT for two systems. In blue we show the results of the single interacting QD (from Fig. 7), and in orange we show the results of the non-interacting DQD (from Fig. 8). As shown, the line-shapes are similar, yet they differ even though both systems can occupy up to two electrons simultaneously, and even though both have two transport channels at the same energy. That being said, the systems differ if one considers the fact that the for the interacting system lower channel of the QD is spin-degenerate. This sort of behavior where degeneracy induces scaling is not unique to our system and has been previously discussed^{54,55}.

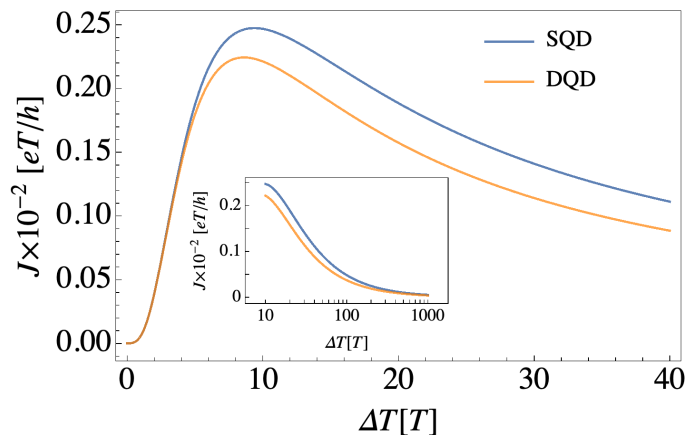


FIG. 9: Current flowing through the system vs. ΔT . The inset shows the same plot but for extremely high temperature difference. Parameter values: $\Gamma = T/20$, $\epsilon_A = 10T$, $\epsilon_B = 40T$, $\mu_L = 28T$, $\mu_R = 22T$.

To conclude, in this example the interaction does not affect the mechanisms described in a unique manner. However, as it affects the number transport channels and their degeneracy and it enables some features which are not predicted in their absence. For instance, setups such as those realized in figures 4(b) and 5, where the systems alternate between harvesting and investing energy cannot be realized in any of the simpler systems discussed in this appendix. This is due to the simple reason that even if we consider an infinitely large thermal bias, the current will not change its sign. Instead it will simply vanish altogether, as at infinite temperature the hot lead Fermi distribution is simply $f = 1/2$ for all energies, which dic-

tates zero current for a system with the same amount of channels which support current in opposite directions. This is seen in the inset of Fig. 9 in which thermal bias is allowed to be ridiculously high resulting in vanishing current.

A more fundamental consequence of interaction is shown in figure 10. Here, we again consider both the non-interacting DQD and the SQD, yet we align the chemical potentials such that the higher channel (ϵ_B or $\epsilon + U$ depending on the system) is within the Fermi window. Figure 10 shows $J(\Delta T)$ for the described setup, and in this setup the fundamental difference between the systems is shown. For the DQD heating the right lead disturbs current flowing via ϵ_B , but for larger ΔT it enables also current flow via ϵ_A which consequently results in non-monotonic line-shape. For the SQD, heating the right lead disturbs current flowing via $\epsilon + U$. However, enabling current flow via ϵ for larger ΔT reduces current flow via $\epsilon + U$ further, such that the overall flow cannot benefit from it.

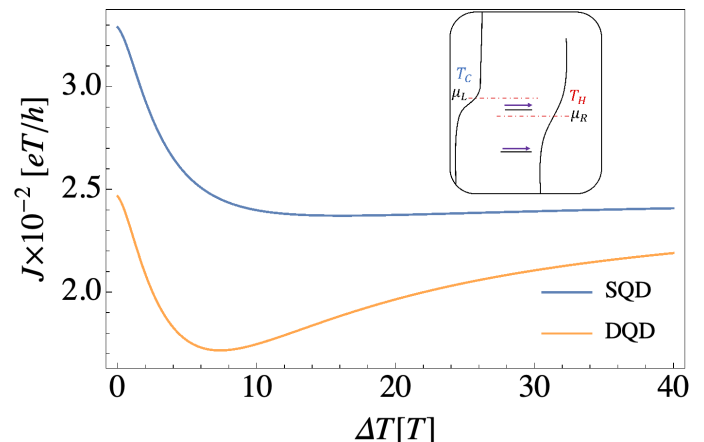


FIG. 10: Current flowing through the system vs. ΔT . The inset illustrates the alignment of transport channels with respect to the chemical potential of the leads. Parameter values: $\Gamma = T/20$, $\epsilon_A = 10T$, $\epsilon_B = 40T$, $\mu_L = 28T$, $\mu_R = 22T$.

Figure 10 shows also two more general phenomena. When aligning the chemical potentials such that one of the channels is within the Fermi window, it is possible to; First, predict non-monotonic current without competition (i.e. current through all channels flows in the same direction). Second, it is possible to predict a local minima for in the magnitude of $J(\Delta T)$. This can also be realized with an interacting system and not just for the non-interacting DQD.

¹ GD Mahan and JO Sofo. The best thermoelectric. *Proceedings of the National Academy of Sciences*, 93(15):7436–7439, 1996.

² MS Dresselhaus, G Dresselhaus, X Sun, Z Zhang, SB Cronin, and T Koga. Low-dimensional thermoelectric materials. *Physics of the Solid State*, 41(5):679–682, 1999.

³ Mildred S Dresselhaus, Gang Chen, Ming Y Tang, RG Yang, Hohyun Lee, DZ Wang, ZF Ren, J-P Fleurial, and Pawan Gogna. New directions for low-dimensional thermoelectric materials. *Advanced materials*, 19(8):1043–1053, 2007.

⁴ Xiaodong Wang and Zhiming M Wang. *Nanoscale ther-*

- moelectrics*, volume 16. Springer, 2014.
- ⁵ Longji Cui, Ruijiao Miao, Chang Jiang, Edgar Meyhofer, and Pramod Reddy. Perspective: Thermal and thermoelectric transport in molecular junctions. *The Journal of Chemical Physics*, 146(9):092201, 2017.
 - ⁶ Giuliano Benenti, Giulio Casati, Keiji Saito, and Robert S Whitney. Fundamental aspects of steady-state conversion of heat to work at the nanoscale. *Physics Reports*, 694:1–124, 2017.
 - ⁷ Dvira Segal. Thermoelectric effect in molecular junctions: A tool for revealing transport mechanisms. *Physical Review B*, 72(16):165426, 2005.
 - ⁸ Yueqi Li, Limin Xiang, Julio L Palma, Yoshihiro Asai, and Nongjian Tao. Thermoelectric effect and its dependence on molecular length and sequence in single dna molecules. *Nature communications*, 7:11294, 2016.
 - ⁹ Roman Korol, Michael Kilgour, and Dvira Segal. Thermopower of molecular junctions: Tunneling to hopping crossover in dna. *The Journal of Chemical Physics*, 145(22):224702, 2016.
 - ¹⁰ C. W. J. Beenakker and A. A. M. Staring. Theory of the thermopower of a quantum dot. *Phys. Rev. B*, 46:9667–9676, 1992.
 - ¹¹ AAM Staring, LW Molenkamp, BW Alphenaar, H Van Houten, OJA Buyk, MAA Mabesoone, CWJ Beenakker, and CT Foxon. Coulomb-blockade oscillations in the thermopower of a quantum dot. *EPL (Europhysics Letters)*, 22(1):57, 1993.
 - ¹² Holger Thierschmann, Rafael Sánchez, Björn Sothmann, Hartmut Buhmann, and Laurens W Molenkamp. Thermoelectrics with coulomb coupled quantum dots. *arXiv preprint arXiv:1603.08900*, 2016.
 - ¹³ Paolo Andrea Erdman, Francesco Mazza, Riccardo Bosisio, Giuliano Benenti, Rosario Fazio, and Fabio Taddei. Thermoelectric properties of an interacting quantum dot based heat engine. *Physical Review B*, 95(24):245432, 2017.
 - ¹⁴ Robert S. Whitney. Most efficient quantum thermoelectric at finite power output. *Phys. Rev. Lett.*, 112:130601, 2014.
 - ¹⁵ Vincent Talbo, Jérôme Saint-Martin, Sylvie Retailleau, and Philippe Dollfus. Non-linear effects and thermoelectric efficiency of quantum dot-based single-electron transistors. *Scientific reports*, 7(1):14783, 2017.
 - ¹⁶ Martin Josefsson, Artis Svilans, Adam M. Burke, Eric A. Hoffmann, Sofia Fahlvik, Claes Thelander, Martin Leijnse, and Heiner Linke. A quantum-dot heat engine operating close to the thermodynamic efficiency limits. *Nature Nanotechnology*, 2018.
 - ¹⁷ D. M. Kennes, D. Schuricht, and V. Meden. Efficiency and power of a thermoelectric quantum dot device. *EPL (Europhysics Letters)*, 102(5):57003, 2013.
 - ¹⁸ David Sanchez and Rosa Lopez. Nonlinear phenomena in quantum thermoelectrics and heat. *Comptes Rendus Physique*, 17(10):1060–1071, 2016.
 - ¹⁹ Holger Thierschmann, Rafael Sánchez, Björn Sothmann, Fabian Arnold, Christian Heyn, Wolfgang Hansen, Hartmut Buhmann, and Laurens W Molenkamp. Three-terminal energy harvester with coupled quantum dots. *Nature nanotechnology*, 10(10):854–858, 2015.
 - ²⁰ Artis Svilans, Adam M. Burke, Sofia Fahlvik Svensson, Martin Leijnse, and Heiner Linke. Nonlinear thermoelectric response due to energy-dependent transport properties of a quantum dot. *Phys. E Low-dimensional Syst. Nanostructures*, 82:34–38, 2016.
 - ²¹ S Fahlvik Svensson, Eric A Hoffmann, Natthapon Nakpathomkun, P M Wu, HQ Xu, Henrik A Nilsson, David Sánchez, Vyacheslavs Kashcheyevs, and Heiner Linke. Nonlinear thermovoltage and thermocurrent in quantum dots. *New Journal of Physics*, 15(10):105011, 2013.
 - ²² Alejandro Marcos-Vicioso, Carmen López-Jurado, Miguel Ruiz-Garcia, and Rafael Sánchez. Thermal rectification with interacting electronic channels: Exploiting degeneracy, quantum superpositions, and interference. *Phys. Rev. B*, 98:035414, 2018.
 - ²³ Björn Sothmann, Rafael Sánchez, and Andrew N Jordan. Thermoelectric energy harvesting with quantum dots. *Nanotechnology*, 26(3):032001, 2015.
 - ²⁴ Miguel A. Sierra, M. Saiz-Bretín, F. Domínguez-Adame, and David Sánchez. Interactions and thermoelectric effects in a parallel-coupled double quantum dot. *Phys. Rev. B*, 93(23):235452, 2016.
 - ²⁵ Wei-Jiang Gong, Cui Jiang, Xiaoyan Sui, and An Du. Thermoelectric properties in a parallel double quantum dot structure modulated by the fano interferences. *Journal of the Physical Society of Japan*, 81(10):104601, 2012.
 - ²⁶ Feng Chi, Jun Zheng, Xiao-Dong Lu, and Kai-Cheng Zhang. Thermoelectric effect in a serial two-quantum-dot. *Physics Letters A*, 375(10):1352–1356, 2011.
 - ²⁷ Gagan Rajput and KC Sharma. Colossal enhancement in thermoelectric efficiency of weakly coupled double quantum dot system. *Journal of Applied Physics*, 110(11):113723, 2011.
 - ²⁸ TA Costi and V Zlatić. Thermoelectric transport through strongly correlated quantum dots. *Physical Review B*, 81(23):235127, 2010.
 - ²⁹ M Tsaousidou and GP Triberis. Thermoelectric properties of a weakly coupled quantum dot: Enhanced thermoelectric efficiency. *Journal of Physics: Condensed Matter*, 22(35):355304, 2010.
 - ³⁰ M Bagheri Tagani and H Rahimpour Soleimani. Thermoelectric effects through weakly coupled double quantum dots. *Physica B: Condensed Matter*, 407(4):765–769, 2012.
 - ³¹ Krzysztof P Wójcik and Ireneusz Weymann. Thermopower of strongly correlated t-shaped double quantum dots. *Physical Review B*, 93(8):085428, 2016.
 - ³² S Donsa, S Andergassen, and K Held. Double quantum dot as a minimal thermoelectric generator. *Physical Review B*, 89(12):125103, 2014.
 - ³³ Zhi-Yong Zhang. Thermopower of double quantum dots: Fano effect and competition between kondo and antiferromagnetic correlations. *Journal of Physics: Condensed Matter*, 19(8):086214, 2007.
 - ³⁴ M Wierzbicki and R Swirkowicz. Influence of interference effects on thermoelectric properties of double quantum dots. *Phys. Rev. B*, 84(7):075410, 2011.
 - ³⁵ Xiaoshuang Chen, H. Buhmann, and L. W. Molenkamp. Thermopower of the molecular state in a double quantum dot. *Phys. Rev. B*, 61:16801–16806, 2000.
 - ³⁶ Piotr Trocha and Józef Barnaś. Large enhancement of thermoelectric effects in a double quantum dot system due to interference and Coulomb correlation phenomena. *Phys. Rev. B*, 85(8):085408, 2012.
 - ³⁷ Wilfred G Van der Wiel, Silvano De Franceschi, Jeroen M Elzerman, Toshimasa Fujisawa, Seigo Tarucha, and Leo P Kouwenhoven. Electron transport through double quantum dots. *Reviews of Modern Physics*, 75(1):1, 2002.
 - ³⁸ Yanchao Zhang, Zhimin Yang, Xin Zhang, Bihong Lin, Guoxing Lin, and Jincan Chen. Coulomb-coupled

- quantum-dot thermal transistors. *EPL (Europhysics Letters)*, 122(1):17002, 2018.
- ³⁹ Martin R Galpin, David E Logan, and Hulikal Ramaiyengar Krishnamurthy. Renormalization group study of capacitively coupled double quantum dots. *Journal of Physics: Condensed Matter*, 18(29):6545, 2006.
- ⁴⁰ Irisnei L Ferreira, PA Orellana, GB Martins, FM Souza, and E Vernek. Capacitively coupled double quantum dot system in the kondo regime. *Physical Review B*, 84(20):205320, 2011.
- ⁴¹ Archak Purkayastha, Abhishek Dhar, and Manas Kulkarni. Out of equilibrium open quantum systems: a comparison of approximate Quantum Master Equation approaches with exact results. *Phys. Rev. A - At. Mol. Opt. Phys.*, 93(6), 2015.
- ⁴² S. Koller, M. Grifoni, M. Leijnse, and M. R. Wegewijs. Density-operator approaches to transport through interacting quantum dots: Simplifications in fourth-order perturbation theory. *Phys. Rev. B*, 82:235307, 2010.
- ⁴³ Yigal Meir and Ned S. Wingreen. Landauer formula for the current through an interacting electron region. *Phys. Rev. Lett.*, 68:2512–2515, 1992.
- ⁴⁴ Gernot Schaller. *Open Quantum Systems Far from Equilibrium*, volume 881 of *Lecture Notes in Physics*. Springer International Publishing, Cham, 2014.
- ⁴⁵ H.P. Breuer and F. Petruccione. *The Theory of Open Quantum Systems*. Oxford University Press, 2002.
- ⁴⁶ Henrik Bruus and Karsten Flensberg. *Many-body quantum theory in condensed matter physics: an introduction*. Oxford University Press, 2004.
- ⁴⁷ S. A. Gurvitz and Ya. S. Prager. Microscopic derivation of rate equations for quantum transport. *Phys. Rev. B*, 53(23):15932–15943, 1996.
- ⁴⁸ Carsten Timm. Tunneling through molecules and quantum dots: Master-equation approaches. *Phys. Rev. B*, 77(19):195416, 2008.
- ⁴⁹ Bingqian Xu and Yonatan Dubi. Negative differential conductance in molecular junctions: an overview of experiment and theory. *Journal of Physics: Condensed Matter*, 27(26):263202, 2015.
- ⁵⁰ Bhaskaran Muralidharan and Supriyo Datta. Generic model for current collapse in spin-blockaded transport. *Phys. Rev. B*, 76:035432, 2007.
- ⁵¹ Miguel A. Sierra and David Sánchez. Strongly nonlinear thermovoltage and heat dissipation in interacting quantum dots. *Phys. Rev. B*, 90(11):115313, 2014.
- ⁵² W. Belzig. Full counting statistics of super-poissonian shot noise in multilevel quantum dots. *Phys. Rev. B*, 71:161301, Apr 2005.
- ⁵³ Padraig Murphy, Subroto Mukerjee, and Joel Moore. Optimal thermoelectric figure of merit of a molecular junction. *Phys. Rev. B*, 78:161406, 2008.
- ⁵⁴ C. W. J. Beenakker. Theory of coulomb-blockade oscillations in the conductance of a quantum dot. *Phys. Rev. B*, 44:1646–1656, 1991.
- ⁵⁵ Giovanni Viola, Sourin Das, Eytan Grosfeld, and Ady Stern. Thermoelectric probe for neutral edge modes in the fractional quantum hall regime. *Phys. Rev. Lett.*, 109:146801, 2012.